AEROSPACE RESEARCH COMMUNICATIONS
ORIGINAL RESEARCH
published: 24 April 2026
doi: 10.3389/arc.2026.15991

Frequency-Dependent Interfacial Instability and Vortex Dynamics of a Disturbed Liquid Jet in Crossflow

Jianfeng Zou[1,2], *Yunfei Hao*[1,2], *Ziting Zhao*[1,2]* and *Jiaqi Sun*[1,2]

[1]School of Aeronautics and Astronautics, Zhejiang University, Hangzhou, Zhejiang, China, [2]Center for Engineering and Scientific Computation, Zhejiang University, Hangzhou, Zhejiang, China

This study investigates the primary atomization dynamics of a sinusoidal-disturbed liquid jet in a gaseous crossflow, focusing on perturbation frequencies spanning 0 – 1500 kHz (Strouhal number St = 0 – 5). A high-fidelity numerical framework combining the Volume of Fluid (VOF) interface capturing method and octree-based adaptive mesh refinement is employed to resolve interfacial instabilities, vortex dynamics, and droplet formation mechanisms. For the undisturbed jet, Rayleigh-Taylor (RT) instability dominates surface wave formation, producing characteristic "Λ"-shaped structures and governing ligament/droplet shedding. Under forced perturbations, four distinct frequencies are systematically analyzed to elucidate modulation effects. Key findings reveal that low-frequency disturbances (St = 0.22) induce periodic flapping, suppress RT-driven waves, and reduce breakup length remarkably, while frequency-matching RT instability (St = 1) amplifies surface undulations, accelerating column disintegration. High-frequency perturbations (St ≥ 2) exhibit rapid near-nozzle damping, restoring unperturbed breakup characteristics. Vorticity analysis identifies counter-rotating vortex pairs as critical drivers of interfacial destabilization, with perturbation frequency non-monotonically modulating annular vortex dynamics. Trajectory comparisons demonstrate breakup length minima at intermediate Strouhal numbers, linked to wavelength-dependent wave topology transitions. These insights establish a frequency-dependent mechanism for controlling jet atomization, offering direct applications for reducing combustion instabilities through targeted flow modulation in propulsion systems.

Keywords: nozzle perturbation, primary breakup, strouhal number, surface structure, VOF method

OPEN ACCESS

***Correspondence**
Ziting Zhao,
12124082@zju.edu.cn

Received: *03 December 2025*
Revised: *06 March 2026*
Accepted: *07 April 2026*
Published: *24 April 2026*

Citation:
Zou J, Hao Y, Zhao Z and Sun J (2026) Frequency-Dependent Interfacial Instability and Vortex Dynamics of a Disturbed Liquid Jet in Crossflow. Aerosp. Res. Commun. 4:15991. doi: 10.3389/arc.2026.15991

INTRODUCTION

The atomization of liquid jets in crossflow (JICF) is a critical process widely employed in aerospace engineering applications, including aero-engine afterburner, ramjet combustor, agricultural spray, etc., which significantly enhances the primary atomization efficiency of the liquid jet [1]. The combustor's combustion efficiency is intricately linked to jet breakup dynamics, as the droplet size distribution and spatial dispersion significantly influence flame stabilization and heat release patterns. Given this critical relationship, establishing predictive computational frameworks capable of resolving interfacial dynamics in multiphase flows remains critical for advancing mechanistic understanding of jet breakup phenomena, constituting a fundamental research priority in fluid dynamics [2].

Numerous experiments and numerical simulations have been conducted to investigate the breakup dynamics of undisturbed liquid jets in crossflow, with particular emphasis on the primary breakup process, vortex structure, jet trajectory and penetration, the mechanism of liquid ligaments and droplets formation, etc., [3]. For breakup mechanism, current understanding attributes the atomization phenomenon primarily to surface waves induced by aerodynamic force. Wu et al. [2] classified the primary breakup characteristics of a non-turbulent liquid jet in a crossflow into column and surface breakup based on gas Weber number We_g and liquid-to-gas momentum ratio q. Furthermore, based on We_g, the column breakup mechanism was further subdivided into four hierarchically organized sub-regimes: (i) enhanced capillary breakup, (ii) bag-type fragmentation, (iii) multimodal disintegration, and (iv) shear-driven atomization. Subsequent researchers have proposed alternative classification methods, such as $We_g - (\lambda_c/d_j)$ and $We_g - (\lambda_s/d_j)$ regime [4], $We_g - Oh$ regime [5], though no universal classification standard has been established to date. Therefore, systematic investigation of jet breakup mechanisms and regime classification remains an unresolved scientific priority.

The breakup process exhibits a highly complex dependence on multiple factors, including nozzle geometry, fluid properties (e.g., density ratio, viscosity, and surface tension), and flow conditions [6, 7]. Conducted early investigations into the effects of the density ratio on the jet breakup process. This study investigated the atomization behavior of a liquid jet in crossflow at low density ratios (r_ρ = 10, 100), revealing that lower density ratios are associated with: (i) reduced liquid core penetration rate, (ii) greater jet bending, and (iii) enhanced lateral expansion. A decrease in density ratio was also found to induce larger column wavelength and average droplet size, whereas the physical mechanism governing liquid fragmentation remained essentially unaltered. Li and Soteriou [8] investigated the impact of density ratio variation on jet breakup morphology through simultaneous adjustments of gas density and velocity while maintaining constant momentum flux ratio and Weber number. Li and Soteriou [9] systematically quantified the effects of high liquid viscosity ($Oh = 0.004 - 2$) on multiple aspects including breakup dynamics, jet penetration depth and trajectory evolution, surface instability development, and droplet size distribution. Nejad and Schetz [10, 11] demonstrated that surface tension exerts negligible influence on jet penetration depth; however, liquids with reduced surface tension exhibited accelerated breakup processes accompanied by reduced droplet sizes.

The aforementioned published studies primarily concentrated on the atomization of undisturbed liquid jet in a uniform crossflow. However, in practical, the acoustic effects generated in unstable engine combustion could affect the fuel atomization process, which provides a feedback mechanism that may dampen or amplify the instability [12]. Therefore, external modulation of the jet, such as introducing pulsation, could serve as an effective strategy to enhance fuel mixing efficiency and reduce combustion instability.

Prior studies on pulsating liquid jets in crossflow configurations have primarily relied on experimental appraoches, with limited exploration through numerical simulations. Elshamy [13], Elshamy et al. [14] investigated the dynamic characteristics of transverse liquid jets in crossflow configurations through simultaneous Mie scattering visualization and particle image velocimetry (PIV), revealing that controlled mechanical excitation profoundly modulates three key processes: (i) fuel-air mixing dynamics, (ii) molecular diffusion mechanisms, and (iii) jet penetration trajectories. The penetration depth can be increased by over 40%, and an optimum excitation Strouhal number of about 0.0047 is obtained, at which a quasi-uniform spray distribution is achieved. Deepe et al. [15] developed a transfer function to characterize the downstream fuel distribution of the pulsating liquid jet through varying the injection frequency of the liquid jet. This function incorporates parameters such as crossflow velocity, mean momentum flux ratio, injection frequency, Weber number, and liquid viscosity. Lee et al. [16] studied the breakup process of a pulsating circular jet injected into a subsonic gaseous crossflow and observed that the imposed pulsation distinctly enhances liquid-gas interfacial mixing through periodic flow destabilization. As pulsation frequency increases, jet penetration depth decreases. Their study examined crossflow velocities ranging from 5 to 143 m/s, with the pulsation frequencies between 35.7 and 166.2 Hz. Furthermore, modulation of transverse gaseous flow velocity has also been investigated. Anderson et al. [17] modified the phase relationship of velocity fluctuations between the crossflow and the fuel to improve the uniformity of the spray field. Their findings demonstrated that potential combustion instabilities could be effectively mitigated by this active control approach. By employing techniques of two-dimensional Mie scattering imaging and laser line Mie scattering measurements, Bunce et al. [12] revealed that the jet penetration height exhibited similarity in both oscillatory and non-oscillatory crossflow. Under oscillatory crossflow condition, the spray displayed a periodic axial motion with a frequency twice that of the main pressure oscillation frequency, especially near the injector. Shaw et al. [18] investigated the atomization of water and Jet A fuel jets in a subsonic crossflow. Experiments were conducted at ambient pressure under two distinct thermal conditions (65 °C and 425 °C), with far-field droplet characteristics measured using PDPA.

The advancement of computational capabilities has enabled the increasing application of numerical simulation techniques to study pulsating liquid jets in crossflow. Zhu et al. [19] investigated the breakup process of a pulsating liquid jet in supersonic crossflow using the CLSVOF method combined with large eddy simulation, with the supersonic airflow modeled as a compressible fluid and the liquid jet as an incompressible fluid, including a gas Mach number of 2, a liquid steady-state velocity of 23 m/s, and sinusoidal pulsation frequencies ranging from 57.5 to 115 kHz. The results of their study showed that the liquid velocity pulsation led to different jet atomization patterns and accelerated the primary breakup process of the liquid jet. The pulsation frequency determined the wavelength of surface wave, and the breakup length of the pulsating jet was shorter than that of the non-pulsating jet, while the penetration depth was greater.

Liu et al. [20] simulated the liquid jet in a supersonic crossflow based on the open-source software AMROC combined with an adaptive mesh refinement algorithm. They analyzed the effects of crossflow Mach numbers and liquid jet velocity pulsations, specifically examining a liquid jet velocity of 15.9 m/s, Mach numbers of 1.5 and 1.8, and a sinusoidal pulsation frequency of 100 kHz. They concluded that pulsation had little effect on penetration depth, but caused additional surface instability and promoted both column and surface breakup of the liquid jet. Although the VOF interface capturing method can precisely calculate the shape of the jet interface and its evolutionary process, it demands a very high grid resolution and a large computational cost, and is still not suitable for spray simulation in real engine combustion chambers. Given the high cost of fully resolving the near-field primary breakup and the downstream droplet characteristics, multi-scale hybrid modeling techniques, specifically the VOF - LPT/DPM coupling method, have been adopted in simulations of liquid jets in crossflow. The fundamental concept is to directly resolve the large-scale gas-liquid interface in the near-nozzle region using a VOF-based two-phase flow method, while in the downstream dilute region, droplets are converted into Lagrangian particles and tracked discretely based on geometric criteria. This approach has been implemented on the OpenFOAM platform by Heinrich et al. [21]. Based on a compressible VOF-LPT coupled solver with adaptive mesh refinement developed in OpenFOAM, Bhatia et al. [22] numerically investigate liquid jet in crossflow breakup under elevated pressures, and analyzed the effects of momentum flux ratio and Weber number on breakup mechanisms. They observed that breakup regimes are governed by different instabilities (Kelvin-Helmholtz and Rayleigh-Taylor) and identified a bifurcation phenomenon at low momentum ratios, attributed to the internal liquid boundary layer and three-dimensional flow field. Sun et al. employed a VOF-LPT coupling method within the Large Eddy Simulation (LES) framework to simulate the column breakup and atomization process of a liquid jet in crossflow, incorporating an interface sub-grid scale term. Their numerical results demonstrated that the inclusion of the liquid Weber number criterion enables an extension of the breakup regime map for JICF. Moreover, the sub-grid scale term was found to significantly influence both the initial evolution of the liquid jet and the droplet size distribution [23]. In their subsequent study, they introduced phase change at the gas-liquid interface and for discrete droplets, and validated the enhanced coupling algorithm using liquid jets in hot air crossflow [24].

Existing studies demonstrate that liquid jet velocity pulsation enhances surface instability, promotes breakup processes, and reduces jet breakup distance. However, its influence on jet penetration depth remains inconsistent across previous investigations. The present study aims to elucidate the interaction mechanisms between perturbed liquid jets and gaseous crossflow, thereby providing a methodology to control and suppress combustion instability growth. Specifically, we focus on the breakup process of liquid jets in crossflow subjected to sinusoidal perturbations at selected frequencies. In prior work, we systematically investigated streamwise forced disturbances affecting liquid ligament and droplet formation mechanisms in circular jets [25] and swirling liquid sheets [26]. Building on these findings, four representative disturbance frequencies were selected for numerical simulations.

The organization of this paper is as follows. Section *Numerical Scheme and Setup* provides the numerical scheme and physical parameters used in present study. In Section *Atomization of Undisturbed Liquid Jet in Crossflow*, the main characteristics of undisturbed liquid jet in a uniform gaseous flow are described, including breakup process, surface instability, and formation of ligaments and droplets. Section *Atomization of Disturbed Liquid Jet in Crossflow* mainly discuss the mechanisms of interaction between the disturbed jet and the transvers gaseous flow, as well as vortex structure, jet trajectory and formation of ligaments and droplets. Finally, important conclusions of present study are provided in Section *Conclusion*.

NUMERICAL SCHEME AND SETUP

Numerical Scheme

In this work, an open-source solver Gerris [27, 28], based on octree and multi-material interface capturing technique, is used to solve the incompressible unsteady Navier-Stokes **Equations 1**, **2**. The solution process includes spatial discretization and time discretization.

$$\frac{\partial(\rho\mathbf{u})}{\partial t} + \nabla\cdot(\rho\mathbf{u}\mathbf{u}) = -\nabla p + \nabla\cdot\mathbf{D} + \sigma\kappa\delta_s\mathbf{n}, \tag{1}$$

$$\frac{\partial\rho}{\partial t} + \nabla\cdot(\rho\mathbf{u}) = 0, \tag{2}$$

where $\mathbf{u} = (u, v, w)$ is the fluid velocity, $\rho = \rho(\mathbf{x}, t)$ is the fluid density, $\mu = \mu(\mathbf{x}, t)$ is the dynamic viscosity, p is the pressure, $\mathbf{D}$ is the viscous stress tensor, defined by **Equation 3**. δ_s is the Dirac distribution function (which means the surface tension is concentrated on the liquid-gas surface), σ is the surface tension coefficient, κ is the mean interface curvature, and $\mathbf{n}$ is the unit normal vector along the interface.

$$\begin{aligned}\mathbf{D} &= 2\mu\mathbf{S} - \frac{2}{3}\mu\nabla\cdot\mathbf{u}\mathbf{I},\\ \mathbf{S} &= \frac{1}{2}\left[\nabla\mathbf{u} + (\nabla\mathbf{u})^{\mathrm{T}}\right].\end{aligned} \tag{3}$$

For two-phase flow, the volume fraction $\alpha = \alpha(\mathbf{x}, t)$ of the first phase is introduced, then the density and viscosity are defined by **Equation 4**:

$$\begin{aligned}\rho &= \alpha\rho_1 + (1-\alpha)\rho_2,\\ \mu &= \alpha\mu_1 + (1-\alpha)\mu_2,\end{aligned} \tag{4}$$

where ρ_1 and ρ_2 denote the densities of the primary and secondary phases, respectively. μ_1 and μ_2 are the dynamic viscosities of the primary and secondary phases, respectively. The convection equation of volume fraction $\alpha(\mathbf{x}, t)$ can be expressed as **Equation 5**:

$$\frac{\partial\alpha}{\partial t} + \nabla\cdot(\alpha\mathbf{u}) = 0. \tag{5}$$

where the phase fraction α is defined as **Equation 6**:

$$\alpha(\mathbf{x},t)=\begin{cases}0 & phase1,\\ 0<\alpha<1 & interface,\\ 1 & phase2\end{cases} \tag{6}$$

The gas–liquid interface is tracked and reconstructed using the Volume of Fluid (VOF) interface capture method. The volume fraction equation is solved for each time step to determine the distribution of volume fractions in the flow field, and then reconstruct the interface information and obtain the flow flux of the grid cells near the interface. The piecewise-linear geometrical Volume-of-Fluid scheme is used for reconstruction [29]. This method achieves second-order accuracy, does not require special treatment of phenomena such as interface breakup and fusion, and effectively captures sharp interface with high precision.

The convection term and diffusion term are discretized by Bell–Colella–Glaz second-order upwind scheme [30] and Crank–Nichoslon scheme [31], respectively.

Moreover, space is discretized by hierarchical quadtree partitioning (octree in 3D) in Gerris. Since jet atomization is a multi-scale physical process, employing a uniform mesh across the entire calculation domain would incur prohibitively high computational costs. Therefore, the Adaptive Mesh Refinement (AMR) method is adopted in the present study to maintain accuracy while minimizing computational cost. By applying interface and vorticity as criteria, the grid is dynamically refined near the interface at each time step, thus ensuring precise tracking of interface deformation.

The accuracy of the numerical method used in this study has been validated in our previous work on swirling liquid sheet [26]. The breakup process of an infinite liquid jet subjected to a small initial disturbance was simulated. The numerical results are in good agreement with the Rayleigh linearized theoretical solution, confirming the model's ability to capture the instability and breakup dynamics of jets.

Numerical Setup

The physical configuration of the base case consists of a liquid diesel fuel stream injected through a circular orifice with diameter $D = 100\,\mu$m into a gaseous crossflow environment. The properties of diesel fuel and the gas are summarized in **Table 1**. The crossflow velocity matches the liquid jet velocity at $U_g = U_l$ =30 m/s. As shown in **Figure 1**, the dimensions of the computational domain is $40D \times 20D \times 10D$. The gaseous flow direction aligns with the positive x axis, while the liquid circular jet propagates along $-y$. A velocity boundary condition is applied to both the gas inlet (left side) and the liquid inlet (upper side), with an outlet boundary condition applied to the right side and symmetric boundary conditions applied to the remaining three boundaries.

To simplify the model and concentrate on the influence of pulsation at the nozzle exit, both gasoues and liquid flow are considered as uniform flows. If turbulence is taken into account, there might exist a coupling or competitive relationship between the disturbance frequency and the turbulent pulsation, which would complicate the causal relationship in the subsequent analysis. In the research conducted by Shinjo and Umemura [32], the inlet velocity was also set as a uniform distribution, and other nozzle interference factors such as turbulence were ignored to establish a clear causal relationship in the analysis. Therefore, for the same reason, an idealized nozzle configuration is adopted in this study.

TABLE 1 | Liquid/gas properties and flow parameters.

Phase	U(m/s)	ρ(kg/m^3)	μ(Pa· s)	σ(N/m)	D(μm)
Liquid	30	848	2.87×10^{-3}	3.0×10^{-2}	100
Gas	30	34.5	1.97×10^{-5}	—	—

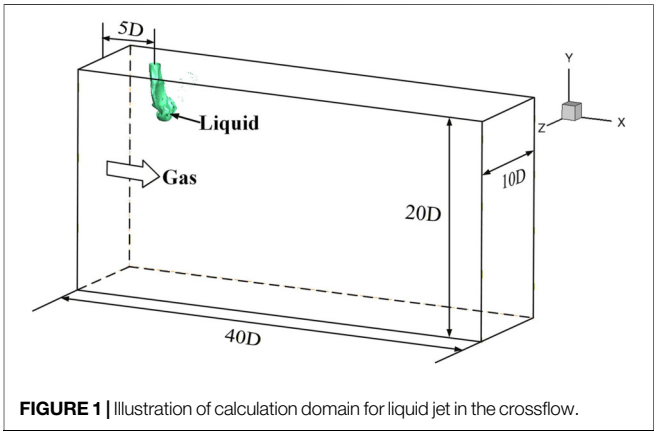

FIGURE 1 | Illustration of calculation domain for liquid jet in the crossflow.

Effect of mesh Resolution and Domain Size

Figure 2 shows the mesh resolution employed in the present study. By appling the interface-basded and vorticity-based refinement criteria, the grid is dynamically refined both at the gas-liquid interface and in regions of high vorticity. In the present study, the minimum grid size used in the calculation is 2 μm [25]. investigated the streamwise forcing effects on the liquid circular jet using a minimum grid size of 2 μm, closely matching the present mesh resolution. Yang and Turan [33] demonstrated that a grid resolution with a minimum scale of 2 μm adequately resolves ligament structures, droplets, and the jet breakup process through comprehensive quantitative and qualitative validation. Given the identical grid resolution adopted in our study, the reliability of the present results is thereby confirmed. In present study, the simulated jet structures and mean jet diameter obtained with the 2 μm minimum grid size demonstrate strong agreement with the existing results in the literature. Additionally, simulations using a coarser grid with a minimum scale of 4 μm were also conducted, and the results were compared in **Figure 3**. From the transient gas-liquid interface profiles and jet trajectories, it is evident that although the jet trajectories achieved with these two grids align closely, the coarse grid fails to accurately resolve surface waves and column breakup effectively. Thus, the 2 μm minimum grid scale adopted in this work better resolves the breakup process.

Building upon the grid independence verification, the authors further examine how domain boundaries affect flow

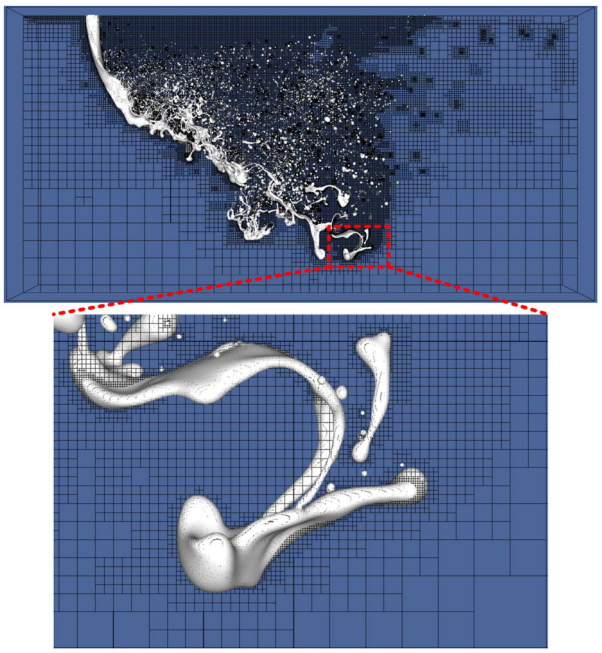

FIGURE 2 | Mesh resolution in present simulation.

characteristics. To investigate the effect of domain size, we conducted additional simulations with an extended computational domain ($50D \times 20D \times 10D$) and compare these results with the baseline case, and the distance between the gas inlet and the center of the circular jet was increased from $5D$ to $15D$. **Figure 4** shows the comparison between the two simulation cases. Based on the gas-liquid profiles in **Figures 4A,B**, the liquid core and large-scale structures closely match. In **Figure 4B**, where the liquid trajectories are compared, the two curves coincide with each other very well. These results demonstrate that the important characteristics of the liquid jet remain unaffected by changing the domain size. Consequently, to avoid excessive computational expense in subsequent simulations, we adopt the smaller domain configuration where the crossflow inlet is positioned $5D$ from the jet centerline.

ATOMIZATION OF UNDISTURBED LIQUID JET IN CROSSFLOW

Overall Structure

In the present study, the key dimensionless parameters are defined and given as follows: the liquid Weber number $We_l = \frac{\rho_l D U_l^2}{\sigma} = 2544$; the gas Weber number

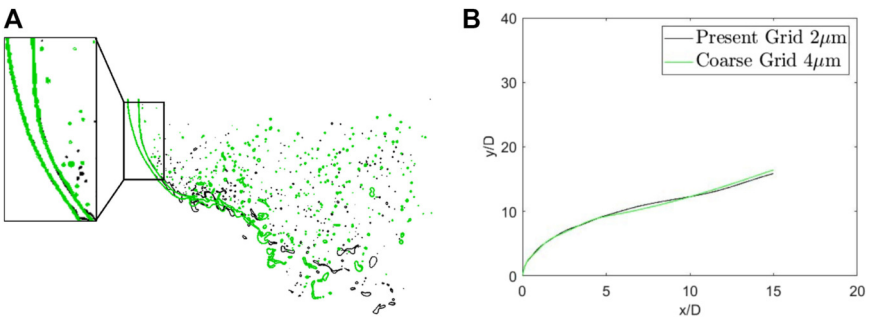

FIGURE 3 | The effect of grid size, the black line presents grid size in present setup, and the green line presents the coarse grid. **(A)** Gas-liquid interface profile, $t = 100\ \mu s$. **(B)** Jet trajectory.

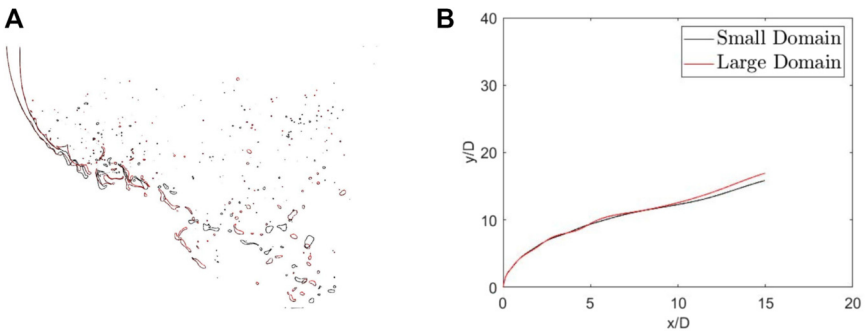

FIGURE 4 | The effect of domain size, the black line presents domain size in present setup, and the red line presents the large computational domain. **(A)** Gas-liquid interface profile, $t = 100\ \mu s$. **(B)** Jet trajectory.

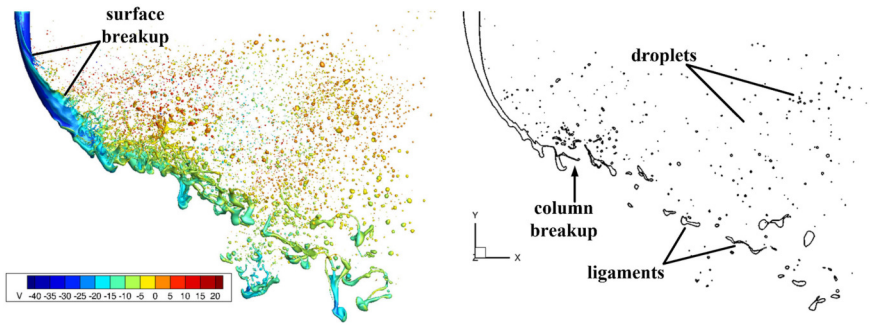

FIGURE 5 | Typical breakup process of undisturbed liquid jet in a gaseous crossflow (time = 96 μs, the color indicates the axial velocity in m/s).

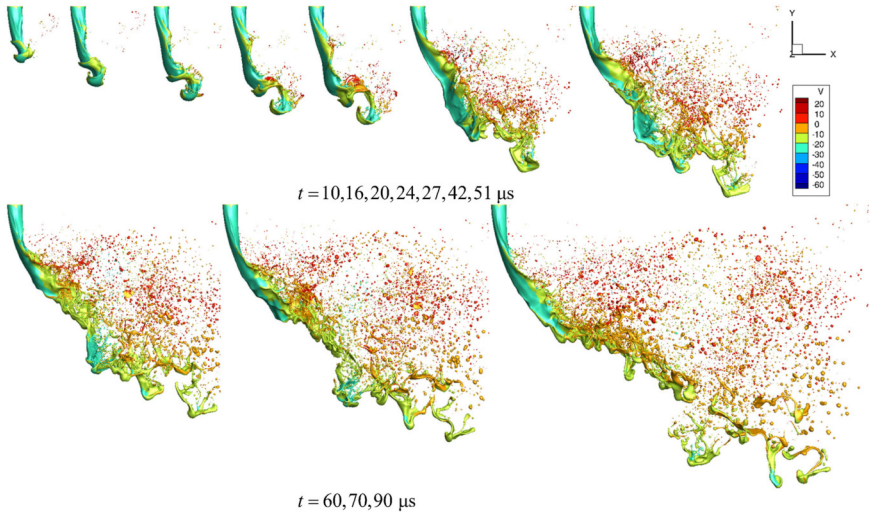

FIGURE 6 | Time evolution of undisturbed liquid jet in a gaseous crossflow (the color indicates the axial velocity in m/s).

$\mathrm{We}_g = \frac{\rho_g D U_g^2}{\sigma} = 103.5$; the liquid-gas momentum flux ratio $q = \frac{\rho_l U_l^2}{\rho_g U_g^2} = 24.58$; and the Ohnesorge number $\mathrm{Oh} = \frac{\mu_l}{(\rho_l D \sigma)^{1/2}} = 0.0569$. According to the primary breakup regime classification proposed by Wu et al. [2], the operating condition in present study lies within the vicinity of the multi-mode and shear breakup transition. It should be noted that previous literature has proposed various classification maps for primary breakup regimes [3]. Wu et al. [2] utilized $\mathrm{We}_g - q$ parameter space for classification, while Mazallon et al. [4] employs $\mathrm{We}_g - \mathrm{Oh}$ as criteria. However, there are currently no universally accepted standard classification criteria, and further research is required to establish consensus.

First, we simulated the undisturbed liquid jet in crossflow, as illustrated in **Figure 5**. The characteristic breakup process of JICF [2] can be clearly identified. The left column of **Figure 5** shows the liquid-gas interface through a contour corresponding to a liquid volume fraction of 0.5, where color mapping indicates axial velocity. **Figure 5** reveals that the axial velocity of the liquid column progressively diminishes with increasing distance from the nozzle, while surface breakup phenomena emerge due to crossflow-induced shear effects. Further, the leeward vortex of the liquid jet redirects droplet velocities towards the $+y$ direction. The right column of **Figure 5**, representing the gas-liquid interface at $z = 0$, demonstrates both column breakup and a large number of ligaments and droplets.

The temporal evolution of a jet in crossflow is illustrated in **Figure 6**, which reveals clear evidence of both surface and column breakup phenomena. Following injection from the nozzle, the jet's leading edge deforms into a mushroom-like structure due to crossflow impingement. Under sustained aerodynamic loading from the gaseous crossflow, the liquid jet core undergoes progressive flattening and curvature development, exhibiting pronounced bending alignment with the crossflow direction. **Figure 7** provides a systematic analysis of cross-sectional deformation dynamics. As the liquid jet propagates downstream, its transverse dimension (along the z-direction) demonstrates progressive expansion, while the cross-sectional geometry gradually transitions from circular to crescent morphology. This geometric transformation enhances windward surface exposure to transverse flow, thereby

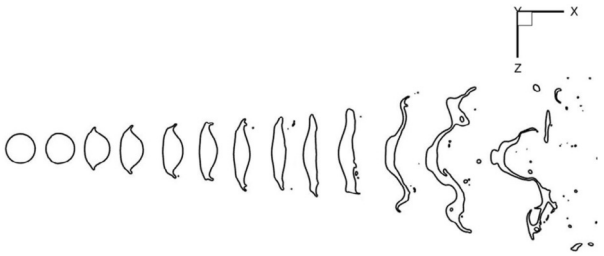

FIGURE 7 | Top view of the deformation of the liquid jet column at various heights from the injector, with intervals of 0.5D (time = 96 μs).

amplifying aerodynamic drag and accelerating liquid column bending. The interaction between high-speed gas flow shear stresses at lateral edges and vortex-induced coiling mechanisms leads to progressive thinning of the liquid film at the periphery. This thinning process culminates in subsequent shedding of ligaments and droplets. Further downstream, the crescent-shaped liquid core gradually reverts to an irregular geometry through dynamic restructuring. A distinctive transverse edge develops on the deformed liquid core, from which secondary ligament and droplet shedding occurs under sustained gas flow shear–a process bearing mechanistic resemblance to secondary droplet breakup phenomena.

It should be emphasized that under the coupled transverse-axial gas flow effects, bag breakup occurs near the liquid jet tip. To clarify this mechanism, **Figure 8** displays the temporal evolution of bag breakup phenomena, with critical stages marked by red arrows. The elevated stagnation pressure on the windward side of the flattened liquid column induces bag formation at its downstream center, where the bag progressively enlarges in the transverse gas flow direction. As shown in **Figure 8**, when approaching maximum expansion, the liquid bag detaches from the column apex through a detachment process analogous to droplet bag breakup. However, according to breakup regime classifications established in existing literature, the dimensionless numbers in the present study deviate from those characterizing conventional bag breakup. Our simulation results demonstrate that local breakup patterns depend not only on the initial global field but also exhibit significant coupling with local flow conditions. Consequently, exclusive reliance on dimensionless numbers for regime classification is inadequate; this finding is crucial for improving atomization modeling accuracy.

Surface Instability

Under the current JICF conditions, we quantify the dominant wavelengths of three competing instability modes–Rayleigh-Taylor (RT), Kelvin-Helmholtz (KH), and capillary instabilities–through theoretical analysis. This wavelength comparison enables definitive identification of the prevailing instability mechanism governing the present JICF breakup process.

RT Instability

The wavelengths corresponding to the maximum growth rate of the RT instability are given by **Equation 7**:

$$\lambda_{R-T,opt} = 2\pi\sqrt{\frac{3\sigma}{(\rho_l - \rho_g)a}}, \tag{7}$$

where a is the magnitude of the acceleration of the liquid phase caused by crossflow resistance. Based on the analysis of Xiao et al. [34], the acceleration of the jet column can be expressed as **Equation 8**:

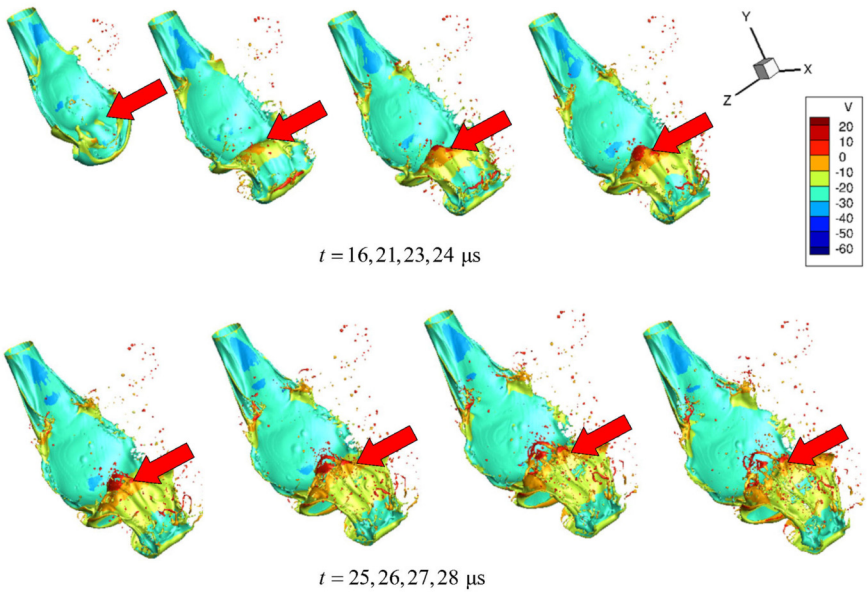

FIGURE 8 | Time evolution of bag breakup (the color indicates the axial velocity in m/s).

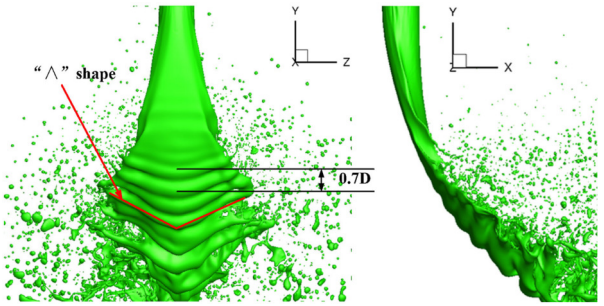

FIGURE 9 | Surface wave structure of undisturbed liquid jet.

$$a = \frac{F}{m} = \frac{C_D \frac{1}{2} \rho_g U_g^2 D_z L_y}{\rho_l \frac{1}{4} \pi D^2 L_y} = \frac{2 C_D \rho_g U_g^2 D_z}{\pi \rho_l D^2}, \tag{8}$$

where C_D is the drag coefficient for the deformed liquid column, D_z is the effective spanwise dimension of the column. The role of capillary instability in column breakup becomes smaller, and RT instability plays a leading role in column breakup.

KH Instability

The dominant wave number of KH instability expressed as **Equation 9** [35]:

$$k_{K-H,opt} = \frac{2 \rho_g \Delta U^2}{3 \sigma}. \tag{9}$$

therefore, the wavelength corresponding to the maximum growth rate of KH instability is obtained as following,

$$\lambda_{K-H,opt} = \frac{2\pi}{k_{K-H,opt}} = \frac{3\pi\sigma}{\rho_g \Delta U^2}. \tag{10}$$

Capillary Instability

The characteristic wavelength induced by capillary instability is given by $\lambda_{Ca,opt} \approx 4.5D$. To identify the dominant instability mechanism governing liquid core breakup under the present operating conditions, **Figure 9** presents the surface wave morphology. Quantitative measurements reveal an initial surface wavelength of approximately 0.7D upstream of the jet, significantly smaller than capillary-driven surface wavelengths resulting from surface tension effects. This comparative analysis confirms that capillary instability does not predominantly govern the liquid core breakup process in our present operation configuration.

Four breakup modes of JICF have been experimentally observed by Sallam et al. [5]. As the gas Weber number increases, the liquid jet progresses through column, bag, multi-mode, and shear breakup regimes sequentially. In the bag breakup mode, the nodal spacing is approximately equal to the jet diameter (D), whereas in the shear breakup mode, the dominant wavelength of disturbance waves reduces to approximately $0.1D$. The present results lie between these two modes (bag and shear breakup modes), approaching the wavelength characteristic of shear breakup, suggesting that the current working condition resides near the multi-mode to shear breakup transition. This observation further validates the accuracy of the present simulation. Sallam et al. [5] additionally identified that disturbance waves emerge upstream of the deflected liquid jet due to Rayleigh-Taylor (RT) instability, which arises from the acceleration of denser fluid into the less dense fluid in this region. To validate this mechanism, we substitute the calculated surface wave acceleration ($a = 6.7 \times 10^5 \mathrm{m/s^2}$) into **Equation 7**, yielding $\lambda_{R-T,opt} \approx 0.8D$, which shows excellent agreement with our simulated wavelength. In contrast, the dominant Kelvin-Helmholtz (KH) instability wavelength calculated from **Equation 10** gives $\lambda_{K-H,opt} \approx 0.2D$. This comparison confirms that RT instability governs the liquid core breakup process under the present conditions. Furthermore, as indicated by red arrows in **Figure 9**, distinctive "Λ"-shaped surface waves are observed to develop on the jet, which can be attributed to the coupled effects of transverse and axial velocity components. This phenomenon, which was also reported by Li and Soteriou [36], provides further validation for the reliability of our computational results.

Formation of Ligaments and Droplets

The evolution of the liquid jet on the windward side is presented in **Figure 10**. Consistent with the analysis in the previous section, increasing distance from the nozzle induces progressive destabilization of the jet surface through Rayleigh-Taylor (RT) instability, resulting in the formation of surface wave structures on the windward side. As shown by black circles in **Figures 10A–I**, airflow-induced stretching causes both sides of the "Λ"-shaped waves to gradually break into ligaments from the troughs. These ligaments subsequently contract and ultimately disintegrate into small droplets, as marked by black circles in **Figures 10J–L**. The bag breakup process in surface wave troughs is highlighted with red circles in **Figure 10**. Transverse airflow generates a high-velocity zone near the lateral edges of surface wave troughs, forcing liquid migration toward the crossflow direction ($+x$) and forming liquid bags. These bags become progressively thinner and eventually develop a central perforation. Subsequent expansion of these perforations leads to the formation of closed ligaments around the holes, as demonstrated by red circles in **Figures 10D–F**. Ultimately, these closed ligaments rupture into striped ligaments, shown by red circles in **Figures 10G–I**.

Ligaments formed through surface wave crest shedding exhibit larger dimensions, consequently producing correspondingly larger droplets. Additionally, as indicated by blue arrows in **Figure 10A**, intense shear effects at the liquid jet's spanwise edge - caused by airflow motion along the surface (z-direction) - induce shear breakup modes. This breakup mechanism generates comparatively smaller droplets.

The aforementioned breakup modes occur periodically near the nozzle. Both bag and shear breakup modes produce relatively small ligaments and droplets, while surface wave crest shedding generates larger ones. Small droplets, characterized by low inertia, experience significant influence from the surrounding flow field, resulting in broad dispersion. Conversely, larger droplets remain predominantly concentrated near the liquid core.

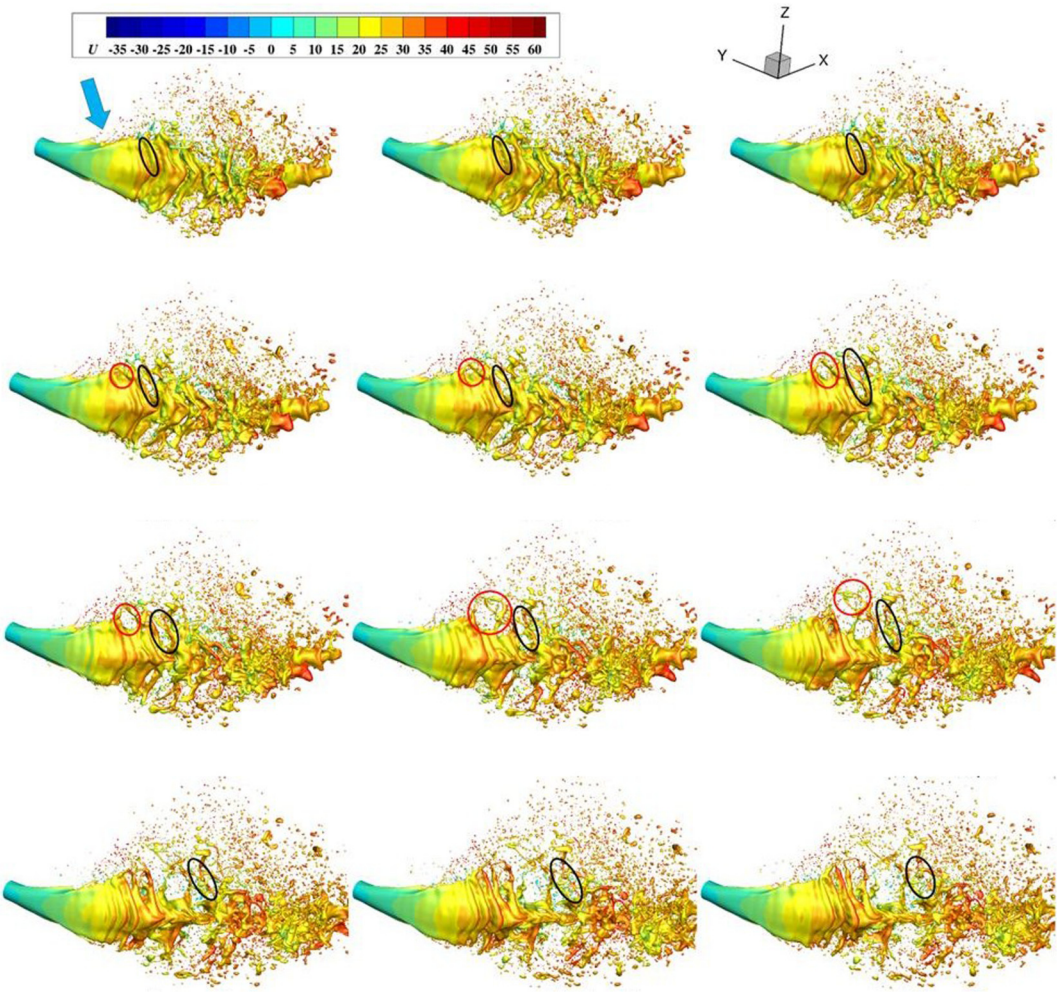

FIGURE 10 | Evolution of the liquid jet on the windward side (the color indicates the *x*-direction velocity in m/s).

ATOMIZATION OF DISTURBED LIQUID JET IN CROSSFLOW

This section analyzes the breakup process of the liquid jet under four sinusoidal perturbation frequencies. The corresponding Strouhal numbers are calculated as $\mathrm{St} = fD/U$, with the disturbance wavelength expressed as $\lambda = \tilde{U}_l/f$, where $\tilde{U}_l$ denotes the liquid jet's mean velocity - defined as the velocity of the undisturbed jet at the nozzle, which is 30 m/s. The wavelength-Strouhal number relationship follows $\lambda/D = 1/\mathrm{St}$. All parameters are summarized in **Table 2**. Case 2's disturbance wavelength corresponds to the capillary instability's dominant wavelength, while Case 3 aligns with the Rayleigh-Taylor (RT) instability's dominant wavelength (see Section *Numerical Scheme and Setup*).

TABLE 2 | Disturbance frequencies and dimensionless parameters of liquid jets.

	f(kHz)	*U*(m/s)	*λ*/*D*	St
Case 1	-	30	-	-
Case 2	66.6	$30[1 + 0.1\sin(2\pi ft)]$	4.5	0.22
Case 3	300	$30[1 + 0.1\sin(2\pi ft)]$	1	1
Case 4	600	$30[1 + 0.1\sin(2\pi ft)]$	0.5	2
Case 5	1,500	$30[1 + 0.1\sin(2\pi ft)]$	0.2	5

Overall Structure

We next analyze and compare the temporal evolution of the disturbed liquid jet under the operating conditions outlined in **Table 2**.

Figure 11 illustrates the temporal evolution of the liquid jet's global structure in Case 2. The liquid column breakup demonstrates a periodic flapping behavior, exhibiting a significantly reduced breakup length relative to undisturbed conditions. Velocity pulsation at the nozzle induces periodic contracting and stretching of the liquid core, resulting in wave node formation. Blue arrows in **Figure 11** track the temporal development of these wave nodes, where spanwise dilatation (z-direction) of the inter-node liquid core occurs due to crossflow-induced aerodynamic forcing. The subsequently

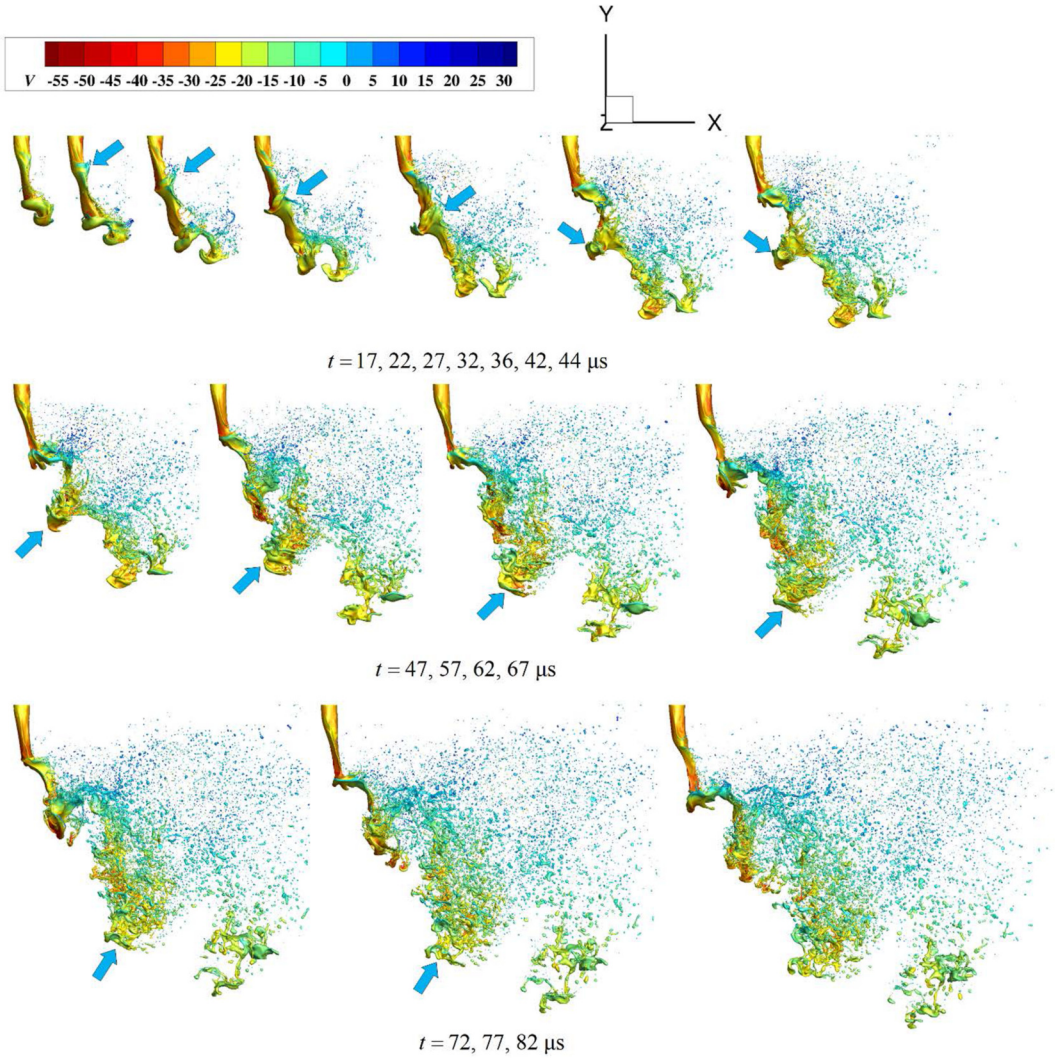

FIGURE 11 | Evolution of the disturbed jet (f = 66.6 kHz, different colors indicate different y-direction velocities (m/s)).

flattened liquid film undergoes thinning until ultimate breaks. This breakup pattern recurs with each pulsation cycle.

Figure 12 shows the temporal evolution of the jet's windward surface viewed along the x-direction. Rayleigh-Taylor (RT) instability-induced fluctuations persist in the planar liquid core between wave nodes. Though, the formation of characteristic undisturbed jet features - specifically, the Λ-shaped surface waves - is prevented by the flow field perturbationthe induced by the pulsed jet. Consequently, no residual spine-like structure remains at this excitation frequency, with jet column disintegration occurring between proximal wave nodes near the nozzle, yielding reduced column breakup length.

Figure 13 presents the temporal evolution of the liquid jet's global structure in Case 3 - where the excitation frequency precisely matches the intrinsic Rayleigh-Taylor (RT) instability frequency - with black lines depicting the gas-liquid interface in the central plane (z = 0). Contrasting with **Figure 12**, periodic flapping breakup of the liquid core is completely absent at this excitation frequency. Nozzle velocity pulsation induces periodic surface fluctuations. Through klystron effect, knot-like liquid structures emerge with sustained wave node amplitude over time. This markedly distinct behavior observed here differs from streamwise-forced circular jet dynamics, where the surface wave on the liquid core, induced by a 300 kHz frequency disturbance, gradually diminishes [25]. The discrepancy originates from distinct dominant breakup mechanisms governing directly injected circular jets versus crossflow liquid jets under identical conditions. Our prior investigations [25] established capillary instability as the primary mechanism governing surface wave dynamics in circular liquid jets. In contrast, the current crossflow jet analysis under undisturbed conditions (Section *Atomization of Undisturbed Liquid Jet in Crossflow*) reveals Rayleigh-Taylor (RT)

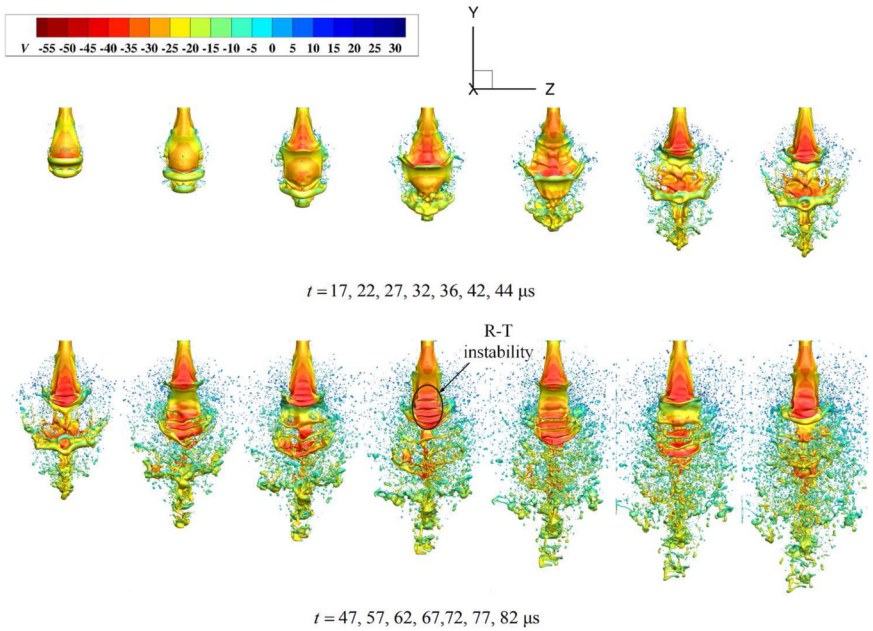

FIGURE 12 | Evolution of the windward side of the disturbed jet (f = 66.6 kHz, different colors indicate different y-direction velocities (m/s)).

instability as the dominant surface destabilization mechanism. This departure in governing physics is also quantitatively evidenced by the characteristic wavelength scaling: the RT-dominant wavelength $\lambda_{R-T} \approx D$ (jet diameter) emerges as significantly smaller than the capillary instability wavelength λ_{Ca}. Such wavelength disparity, coupled with experimental observations of λ_{R-T}-scale wave patterns, fundamentally explains the contrasting interfacial evolution between circular and crossflow jet systems under equivalent perturbation frequencies. Specifically, the amplitude of the surface waves on the transverse jet induced by the disturbance does not exhibit significant attenuation, whereas the amplitude of the surface waves on the circular jet exhibits gradual decay.

Figure 14 illustrates the temporal evolution of the liquid jet's global structure in Case 4. Distinct surface wave structures remain observable in the immediately adjacent jet segment to the nozzle under this specific excitation frequency. Comparative analysis with **Figure 13** indicates that surface waves excited at this characteristic frequency exhibit shorter relative wavelengths. Furthermore, their amplitudes display progressive decay along the jet development, particularly within the near-nozzle region. This behavior aligns closely with previous circular jet observations under equivalent pulsation frequencies [25]. In contrast to the amplitude attenuation observed near the nozzle, surface waves exhibit amplitude recovery in downstream regions ($x/D > 2.5$), demonstrating RT instability's predominance over capillary effects. These transitional zones are explicitly identified in **Figure 15** through solid/dashed red enclosures.

Figure 16 documents the temporal evolution of the liquid jet's global structure in Case 5. While nozzle exit velocity pulsations generate localized perturbations within the proximal jet region ($x/D < 0.5$), capillary-driven damping rapidly dissipates these short-wavelength disturbances. Consequently, the jet's flow morphology beyond ($x/D > 0.5$) closely matches the unperturbed scenario. Crucially, the temporal evolution maintains correspondence with crossflow jet behavior under undisturbed conditions. Surface waves exhibiting the characteristic "Λ"-shape are preserved under this perturbation regime, as identified by black trajectories in **Figure 16**. This demonstrates crossflow liquid jet breakup's insensitivity to high-frequency pulsations, consistent with circular jet observations reported by Zhou et al. [25].

Vortex Structure

The vortical structures inherent to transverse jets (JICF) - encompassing counter-rotating vortex pairs, upright vortices, shear-layer vortices, horseshoe vortices, and wake vortices [37] - serve as critical determinants of liquid jet disintegration, particularly under turbulent jet regimes. These turbulent vortex configurations exert direct control over interfacial instability initiation mechanisms [34]. Given the heightened susceptibility of jet vorticity fields to external perturbations, nozzle-introduced velocity fluctuations considerably modify transverse jet vortex formation dynamics, thereby governing both initial interface destabilization and subsequent breakup processes. This causality necessitates systematic investigation of nozzle perturbation-induced vortex evolution. Among these vortical features, annular and wake vortices play a dominant role in instability initiation, as evidenced by their persistent manifestation in transient flow regimes [38]. Subsequent analysis focuses on perturbation-induced evolution of these two vortex classes.

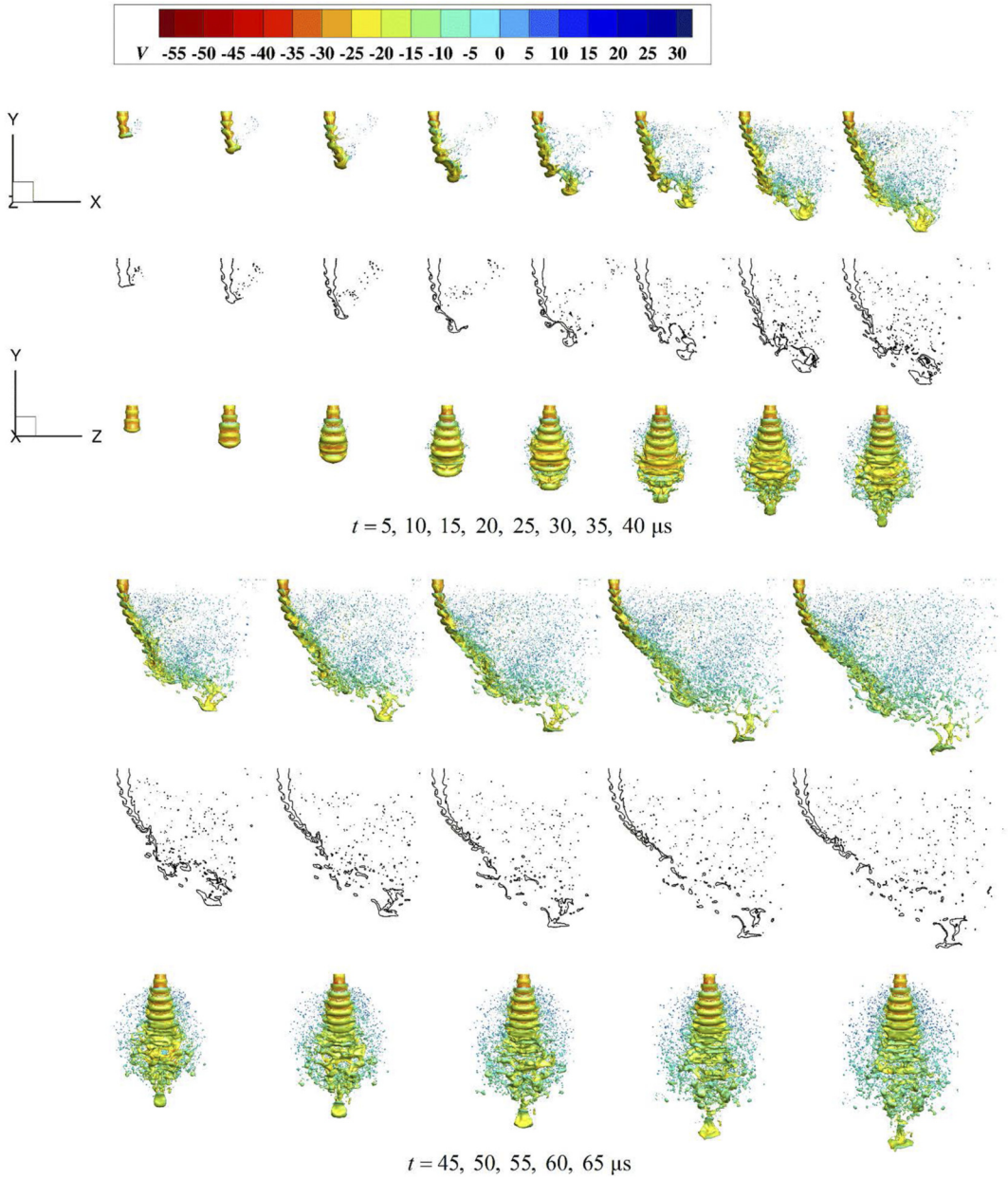

FIGURE 13 | Evolution of the disturbed jet (f = 300 kHz, different colors indicate different y-direction velocities (m/s)).

Figure 17A depicts the instantaneous vortical topology visualized through the Q-criterion, where the velocity field is normalized by the initial jet velocity. The three-dimensional vortex features surrounding the liquid column reveals two dominant structural components: 1) Counter-rotating vortex pairs (CVPs) aligned parallel to the liquid column axis, directly linked to surface breakup mechanisms; and 2) Windward-side vortices governing the onset of interfacial instability. Additionally, as shown in **Figure 17A**, the spatiotemporal evolution of wake, vertical, and droplet-associated vortices critically modulates both mixing efficiency and atomization dynamics. Notably, analogous vortical configurations observed in supersonic transverse jets [19] reveal mechanistic similarities in atomization processes across flow regimes.

Figure 17 documents the perturbation-modulated vortical structures surrounding the jet under multiple excitation conditions. Nozzle-imposed disturbances induce significant modifications to the vortex formation dynamics. The windward annular vortex structure demonstrates non-monotonic scaling with increasing actuation frequency, exhibiting initial expansion followed by subsequent

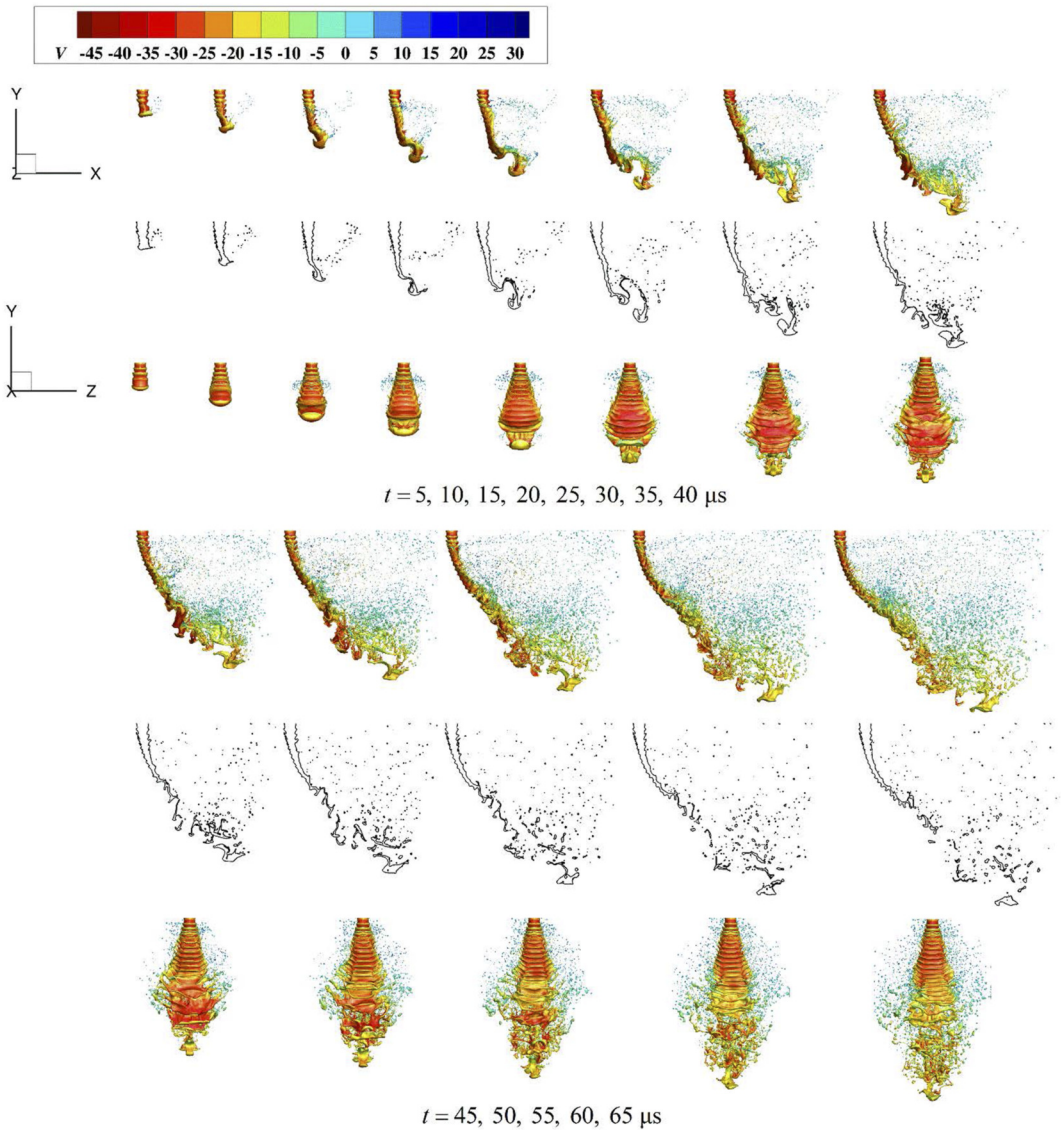

FIGURE 14 | Evolution of the disturbed jet (f = 600 kHz, different colors indicate different y-direction velocities (m/s)).

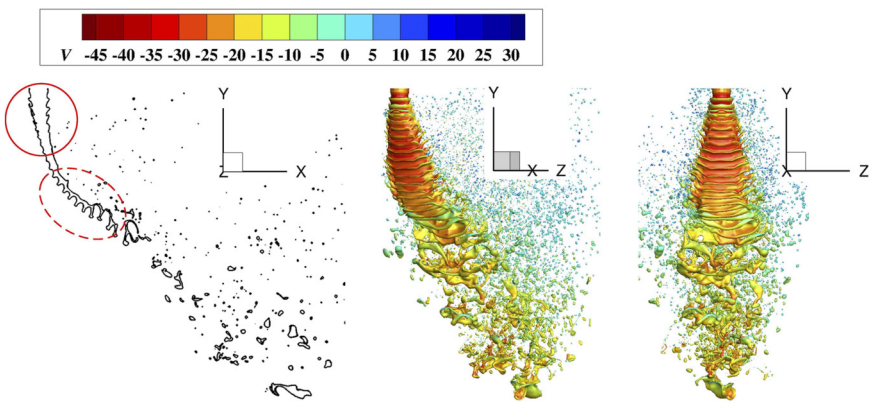

FIGURE 15 | Surface instability of liquid core (f =600kHz, t = 72 μs, different colors indicate different y-direction velocities (m/s)).

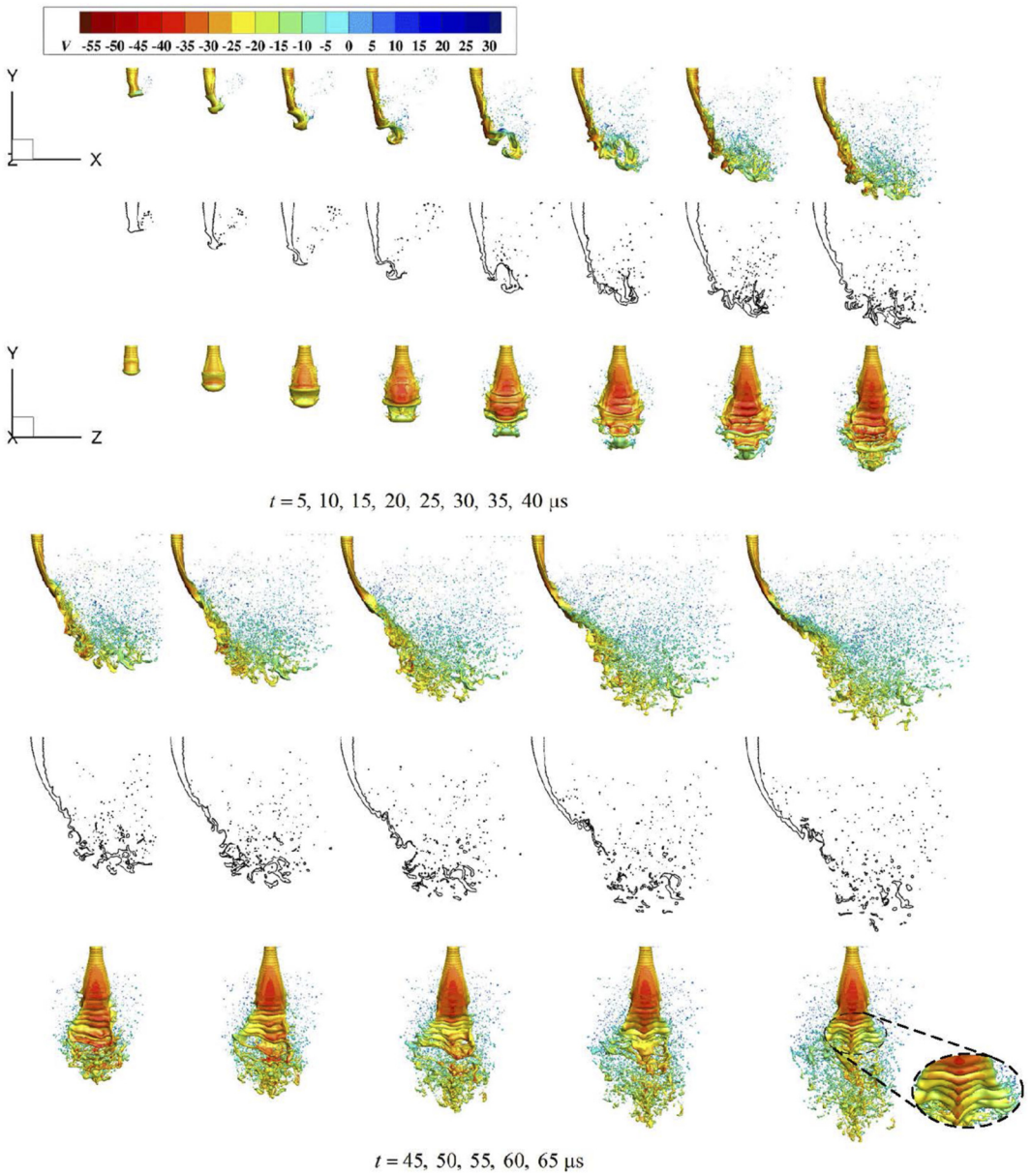

FIGURE 16 | Evolution of the disturbed jet (f = 1500 kHz, different colors indicate different y-direction velocities (m/s)).

contraction. At elevated frequencies, the jet's vortical configuration approximates undisturbed baseline conditions, demonstrating constrained influence of high-frequency perturbations on breakup mechanisms.

Comparison of Jet Penetration and Trajectory

Figure 18 compares windward surface morphologies under varying perturbation frequencies. The unperturbed jet exhibits extended breakup length, where symmetry-preserving waves on the windward interface generate an elongated spine-like liquid ligament along the symmetry plane, deflecting toward the crossflow to enhance liquid core extension. Nozzle-imposed perturbations induce non-monotonic breakup length evolution: initial reduction followed by subsequent elongation with increasing frequency. When surface wavelengths approach RT instability's dominant scale ($f = 0 - 300$kHz), intensified perturbation effects progressively suppress both surface undulations and spinal ligament formation, reducing breakup length through periodic wave packet shedding. However, arrow-marked features in **Figure 18D** reveal trapezoidal wave configurations emerging at f =600kHz, triggering renewed breakup length enhancement. At ultrahigh frequencies

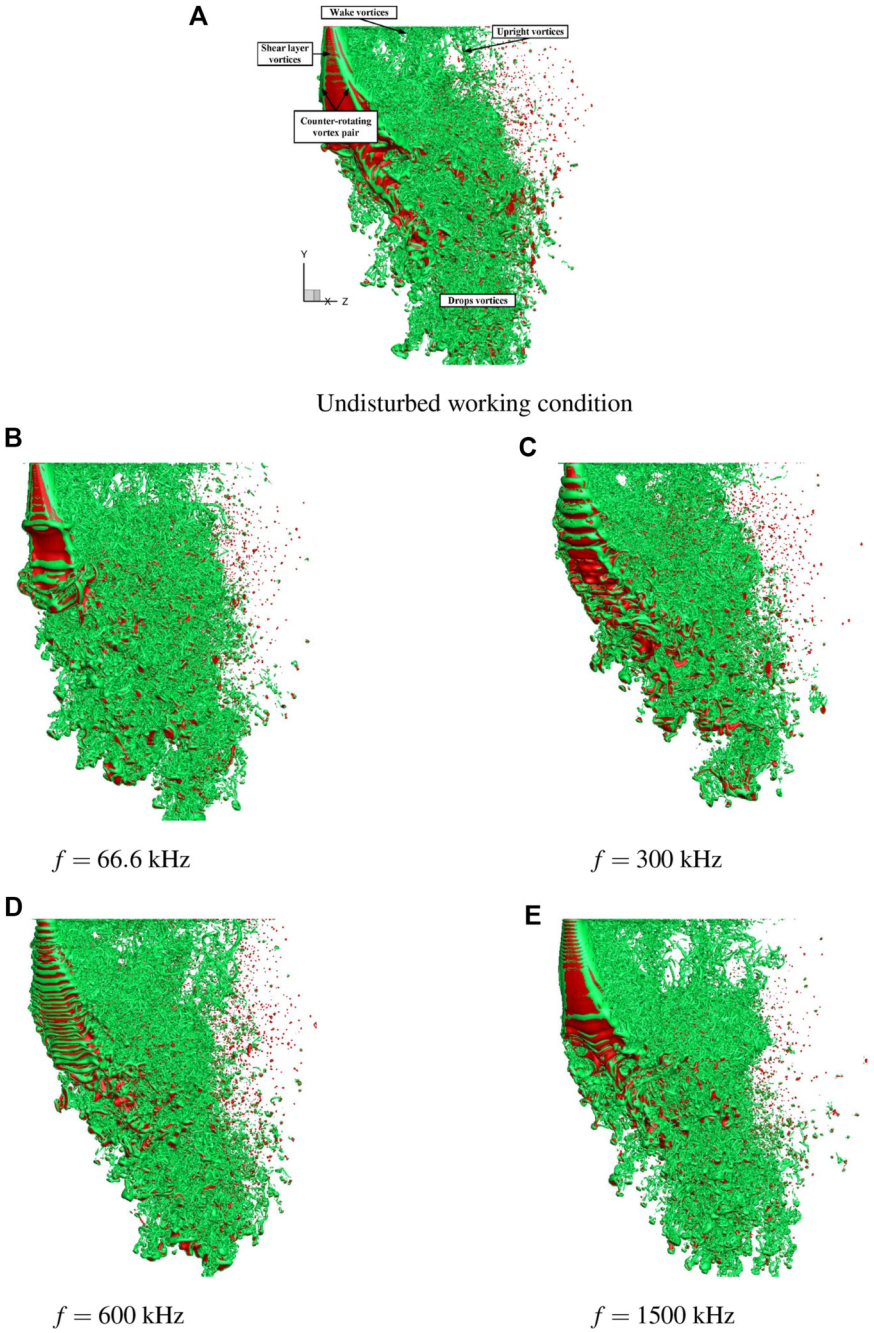

FIGURE 17 | Contour of second invariant of the velocity gradient tensor Q = 500 and liquid jet structure in different disturbed working condition (t = 87 μs). **(A)** Undisturbed working condition. **(B)** f = 66.6 kHz. **(C)** f = 300 kHz. **(D)** f = 600 kHz. **(E)** f = 1500 kHz.

(f =1500 kHz), nozzle-induced wave effects diminish, permitting RT instability-dominated breakup with reemerging "Λ"-shaped waves. This regime restores symmetry-plane liquid ligament deflection and breakup length characteristics analogous to unperturbed conditions.

Subsequent analysis focuses on central plane ($z = 0$) morphological evolution to examine disturbance frequency effects on jet trajectory (**Figure 19**). When the excitation frequency falls below the capillary instability's dominant wavelength threshold (f = 66.6kHz), three distinctive alterations emerge in the perturbed jet compared to its unperturbed counterpart: 1) reduction in breakup length, 2) shortening of column breakup timescale, and 3) periodic lateral oscillations of jet trajectory about its mean path. These collectively enhance crossflow-directed (x-direction) dispersion of ligaments and droplets. Near RT instability's critical frequency

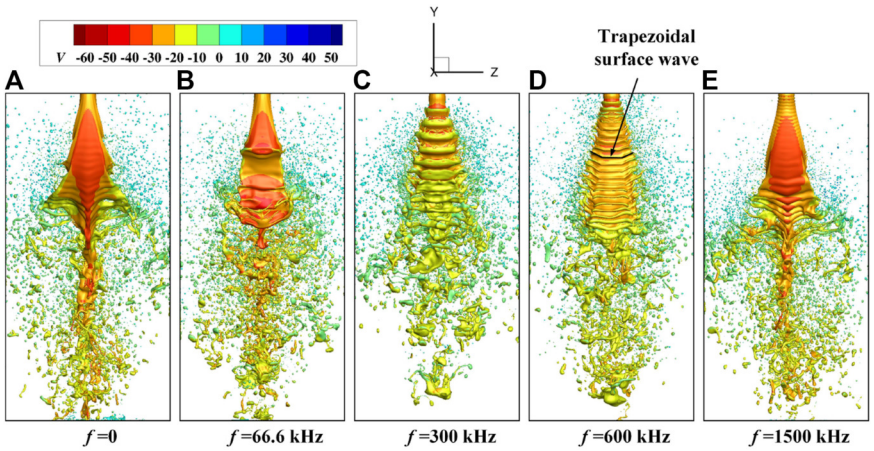

FIGURE 18 | Compare of windward surface of the liquid jet under different disturbance frequencies, from left to right: f = 0, 66.6, 300, 600, 1500kHz (t = 87 μs, different colors indicate different y-direction velocities (m/s)). **(A)** f = 0. **(B)** f = 66.6 kHz. **(C)** f = 300 kHz. **(D)** f = 600 kHz. **(E)** f=1500 kHz.

(f = 300kHz), accelerated surface wave growth induces marked crossflow deflection (**Figure 20**), resulting in earlier breakup of the jet column. At elevated frequencies (f = 600, 1500kHz), breakup length restoration occurs alongside trajectory convergence toward unperturbed characteristics. This non-monotonic breakup length response - initial decrease followed by recovery - reaches minimum values below RT instability's characteristic frequency. The underlying mechanism involves disturbance-induced wavelength modulation: Sub-RT-scale wavelengths transform "Λ"-shaped waves into linear configurations while suppressing spinal ligaments, yielding abrupt breakup length reduction. Super-RT wavelengths generate trapezoidal wave morphologies that delay breakup. Ultimately, high-frequency perturbations (f > 1500kHz) experience rapid near-nozzle attenuation, restoring both "Λ"-shaped wave patterns and breakup characteristics analogous to unperturbed jets.

The trajectory and penetration depth of liquid jets in crossflow (JICF) constitute critical performance metrics, governing fuel distribution patterns within combustion chambers and consequently determining evaporation rates and oxidizer mixing efficiency [3]. This necessitates rigorous quantitative characterization of both jet trajectory and breakup location. Existing predictive formulations, categorized by operating condition regimes such as standard temperature and pressure (STP), high-pressure and standard temperature (STHP), standard pressure and high-temperature (HTSP), and high temperature and pressure (HTP), along with dimensionless parameters including the momentum flux ratio, Weber number, viscosity ratio, and Reynolds number [3], exhibit inherent limitations. Current models split into formulations for unity nozzle discharge coefficients versus sub-unity cases, yet all require experimental calibration for trajectory prediction accuracy. Direct numerical simulations precisely eliminate flow disturbances within nozzle geometries and experimental measurement noise, enabling more reliable revelation of the underlying physical mechanisms governing jet breakup processes. While their idealized boundary conditions require complementary validation through experimental datasets, the high-fidelity numerical results provide critical theoretical foundations for establishing predictive models of jet trajectory evolution.

The trajectory depth of non-disturbed (unperturbed) liquid jets has been comprehensively characterized through well-established empirical correlations in the technical literature. A survey of published models reveals numerous correlations proposed to link trajectory depth with governing parameters including momentum ratio. However, as demonstrated in our cross-comparative analysis (**Figure 21**), significant discrepancies exist among existing trajectory depth prediction models. This pronounced divergence strongly suggests that trajectory depth cannot be uniquely determined by momentum ratio alone but depends on additional dimensionless parameters whose functional relationships remain poorly understood. Through systematic evaluation against our DNS dataset, the multi-parameter framework proposed by Eslamian et al. [39] emerges as the optimal predictor, exhibiting excellent agreement with numerical simulations in trajectory depth quantification. This model, rigorously selected from existing formulations through comparative analysis, achieves near-perfect alignment with DNS-derived penetration profiles, confirming its superior predictive accuracy. The Eslamian correlation, expressed as **Equation 11**:

$$\frac{y}{D} = 0.191\left(\frac{x}{D}\right)^{0.43} q^{0.30}\mathrm{Re}_{\mathrm{ch}}^{0.12}\mathrm{Re}_{l}^{0.14}, \tag{11}$$

where $\mathrm{Re}_{\mathrm{ch}}$ designates the gas-phase Reynolds number based on channel hydraulic diameter, and Re_l corresponds to the liquid-phase Reynolds number normalized by jet diameter. Distinct from conventional formulations, this framework incorporates two critical dimensionless parameters: $\mathrm{Re}_{\mathrm{ch}}$ and Re_l. These

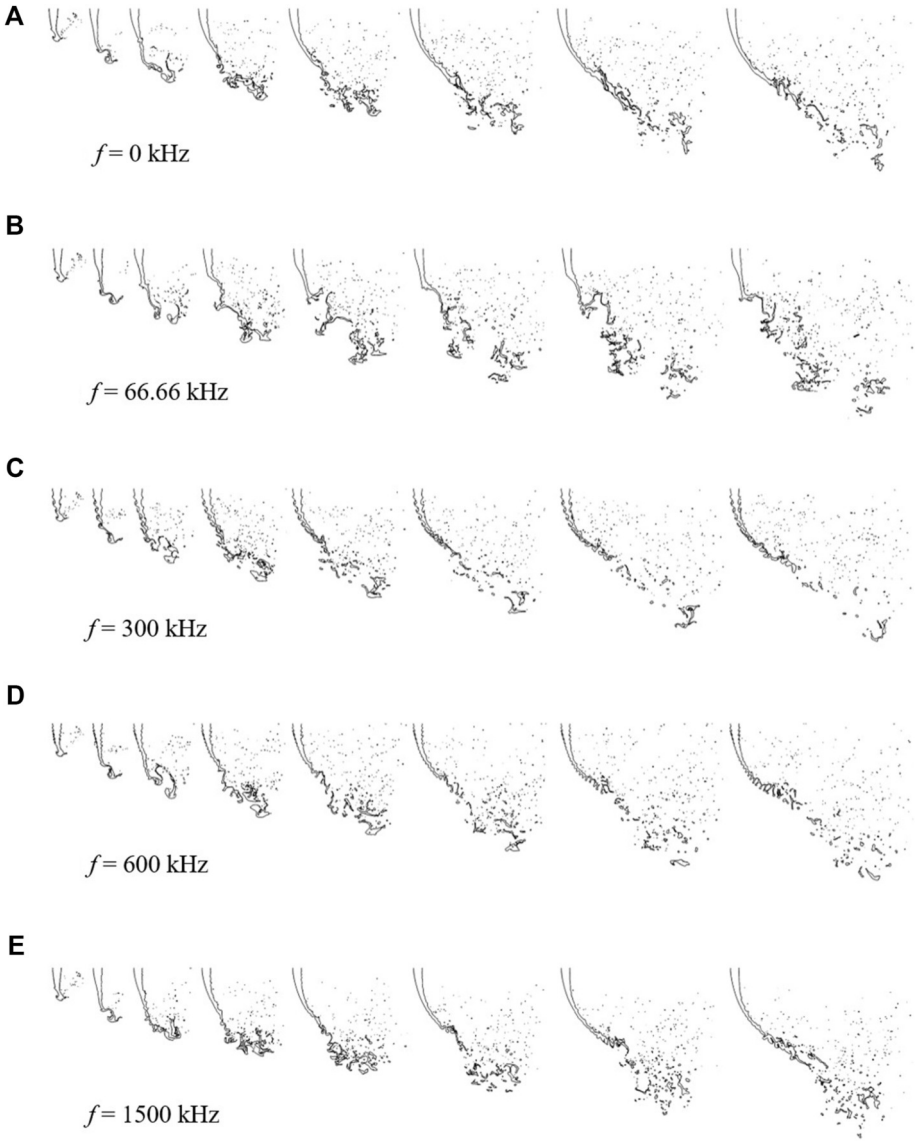

FIGURE 19 | Time evolution of the jet trajectory under different disturbance frequencies (t = 10, 20, 30, 40, 50, 60, 70, 80 μs). **(A)** f = 0 kHz. **(B)** f = 66.6 kHz. **(C)** f = 300 kHz. **(D)** f = 600 kHz. **(E)** f = 1500 kHz.

findings establish that the momentum flux ratio constitutes only one component of jet trajectory determination, necessitating inclusion of additional scaling parameters - a critical requirement emphasized by Chai et al. [38].

The existing predictive models for jet trajectory depth, as discussed above, are principally applicable to either unperturbed liquid jets or those subjected to high-frequency excitation. However, in low-frequency excitation regimes, our detailed analysis reveals that inlet perturbations at the nozzle exert significant influence on both the modal characteristics of surface wave formation and their subsequent development dynamics. Under such perturbed excitation conditions, the resultant jet trajectories and breakup lengths exhibit pronounced unsteady characteristics and nonlinear behavior dominated by multimodal interactions. Consequently, establishing reliable predictive frameworks for jet trajectory and breakup length in low-frequency excitation scenarios requires systematic investigations encompassing broader parametric ranges of excitation characteristics–a critical research gap that constitutes the focus of our planned investigations.

CONCLUSION

This study systematically investigates the primary atomization of a sinusoidal-disturbed liquid jet in a gaseous crossflow across perturbation frequencies spanning 0–1500 kHz (Strouhal

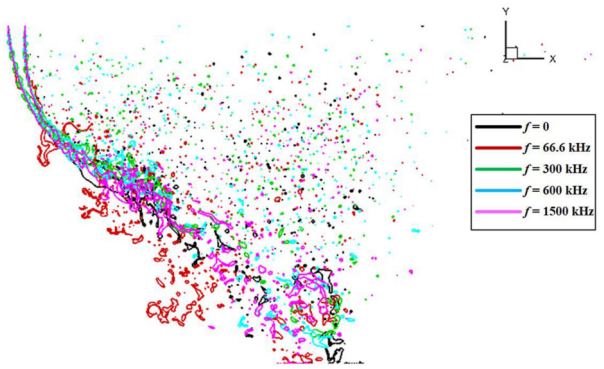

FIGURE 20 | Superposition of jet trajectories in the central plane of the jet for different nozzle disturbance frequencies (different colors indicate different y-direction velocities (m/s)).

number St = 0 – 5) using a high-resolution numerical framework. The key findings are summarized as follows:

1. Undisturbed Jet Dynamics: The column breakup process in unperturbed conditions is governed by Rayleigh-Taylor (RT) instability, with the dominant wavelength ($\lambda_{R-T,opt} \approx 0.8D$) dictating the scale of ligaments and droplets. The interaction of transverse and axial flows generates characteristic "Λ"-shaped surface waves, from which ligaments detach periodically. These ligaments, comparable in size to the RT wavelength, serve as the primary source of large droplets in the spray field. A persistent spine-like liquid band forms along the jet's symmetry plane, enhancing core penetration before eventual disintegration.
2. Frequency-Modulated Breakup: Perturbation frequency critically alters surface wave morphology and breakup length. At low frequencies (St = 0.22), periodic flapping suppresses RT-driven waves, reducing breakup length. When the excitation frequency matches the intrinsic RT instability (St = 1), amplified surface undulations accelerate column fragmentation. High-frequency disturbances (St ≥ 2) exhibit rapid near-nozzle damping, restoring unperturbed "Λ"-shaped waves and breakup characteristics. The breakup length follows a non-monotonic trend, reaching minima at intermediate St due to transitions in wave topology: "Λ"-shaped → linear → trapezoidal → "Λ"-shaped.
3. Jet Trajectory and Modeling Implications: While the gas-liquid momentum flux ratio remains a key parameter for trajectory prediction, turbulent effects and perturbation frequency significantly influence jet dynamics. Existing empirical models relying solely on show poor accuracy, whereas formulations incorporating gas-phase Reynolds number (Re_{ch}) and liquid-phase Reynolds number (Re_l) align closely with simulations. Notably, nozzle-imposed disturbances introduce transient trajectory oscillations, highlighting the need for frequency-dependent corrections in predictive frameworks.

These findings establish a mechanistic link between perturbation frequency, interfacial instability, and atomization efficiency, providing actionable insights for combustion instability reduction. By tailoring excitation frequencies to target specific instability modes (e.g., suppressing RT waves at St = 0.22), active flow control strategies can optimize spray uniformity and mixing in propulsion systems. Future work should expand parametric ranges (e.g., higher We_g, viscosity effects) and integrate frequency modulation into reduced-order models for real-time combustion control. Additionally, subsequent studies will focus on more in-depth quantitative analysis, primarily including: the growth characteristics of unstable waves, the evolution mechanisms of vortex dynamics, and a comprehensive analysis of droplet characteristics across the entire spray field.

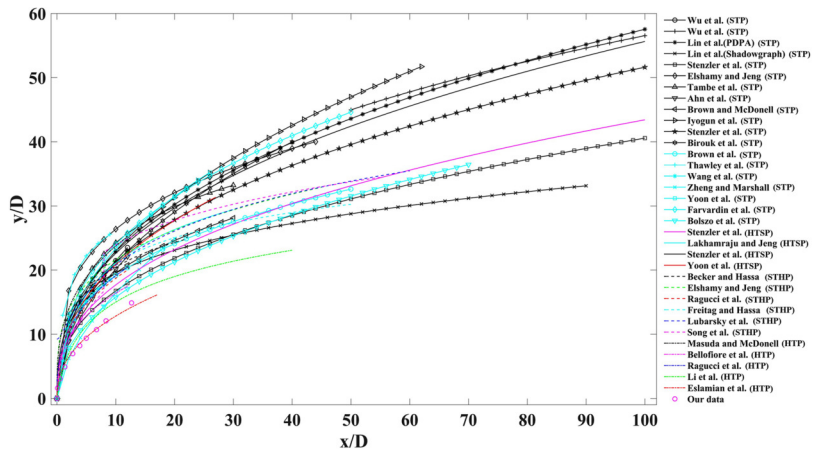

FIGURE 21 | Comparison of the jet trajectory presented in different literature and the simulation result in present study.

DATA AVAILABILITY STATEMENT

The raw data supporting the conclusions of this article will be made available by the authors, without undue reservation.

AUTHOR CONTRIBUTIONS

The first author, JZ, funding acquisition, project administration, supervision and numerical computation. The second author, YH, numerical computation, scientific drawing and draft writing. The third author, ZZ, investigation, methodology and draft writing. The fourth author, JS, investigation and methodology. All authors contributed to the article and approved the submitted version.

FUNDING

The author(s) declared that financial support was received for this work and/or its publication. This research was funded by the National Science and Technology Major Project grant number J2019-III-0004-0047, the National Science and Technology Major Project grant number 2019-III-0014-0058 and the National Natural Science Foundation of China grant number 12172329.

CONFLICT OF INTEREST

The authors(s) declared that this work was conducted in the absence of any commercial or financial relationships that could be construed as a potential conflict of interest.

GENERATIVE AI STATEMENT

The author(s) declared that generative AI was not used in the creation of this manuscript.

Any alternative text (alt text) provided alongside figures in this article has been generated by Frontiers with the support of artificial intelligence and reasonable efforts have been made to ensure accuracy, including review by the authors wherever possible. If you identify any issues, please contact us.

REFERENCES

1. Prakash R, Jain S, Tomar G, V R, Bn R. Computational Study of Liquid Jet Breakup in Swirling Cross Flow. In: *18th Annual Conference on Liquid Atomization and Spray Systems - Asia* (2016).
2. Wu P-K, Kirkendall KA, Fuller RP, Nejad AS. Breakup Processes of Liquid Jets in Subsonic Crossflows. *J Propulsion Power* (1997) 13:64–73. doi:10.2514/2.5151
3. Broumand M, Birouk M. Liquid Jet in a Subsonic Gaseous Crossflow: Recent Progress and Remaining Challenges. *Prog Energy Combustion Sci* (2016) 57:1–29. doi:10.1016/j.pecs.2016.08.003
4. Mazallon J, Dai Z, Faeth GM. Primary Breakup of Nonturbulent Round Liquid Jets in Gas Crossflows. *Atomization and Sprays* (1999) 9:291–312. doi:10.1615/atomizspr.v9.i3.40
5. Sallam KA, Aalburg C, Faeth GM. Breakup of Round Nonturbulent Liquid Jets in Gaseous Crossflow. *AIAA J* (2004) 42:2529–40. doi:10.2514/1.3749
6. Herrmann M. The Influence of Density Ratio on the Primary Atomization of a Turbulent Liquid Jet in Crossflow. *Proc Combustion Inst* (2011) 33:2079–88. doi:10.1016/j.proci.2010.07.002
7. Herrmann M, Arienti M, Soteriou M. The Impact of Density Ratio on the Liquid Core Dynamics of a Turbulent Liquid Jet Injected into a Crossflow. *J Eng Gas Turbines Power* (2011) 133:061501. doi:10.1115/1.4002273
8. Li X, Soteriou MC. Detailed Numerical Simulation of Liquid Jet Atomization in Crossflow of Increasing Density. *Int J Multiphase Flow* (2018) 104:214–32. doi:10.1016/j.ijmultiphaseflow.2018.02.016
9. Li X, Soteriou M. Investigation of the Impact of High Liquid Viscosity on Jet Atomization in Crossflow Via high-fidelity Simulations. *Phys Fluids* (2017) 29:082103. doi:10.1063/1.4996178
10. Nejad AS, Schetz JA. Effects of Properties and Location in the Plume on Droplet Diameter for Injection in a Supersonic Stream. *AIAA J* (1983) 21:956–61. doi:10.2514/3.8183
11. Nejad AS, Schetz JA. Effects of Viscosity and Surface Tension on a Jet Plume in Supersonic Crossflow. *AIAA J* (1984) 22:458–9. doi:10.2514/3.8421
12. Bunce K, Lee J, Santavicca D. Characterization of Liquid jets-in-crossflow Under High Temperature, High Velocity Non-oscillating and Oscillating Flow Conditions. In: *44th AIAA Aerospace Sciences Meeting and Exhibit*, 20. (2006). doi:10.2514/6.2006-1225
13. Elshamy O. Experimental Investigations of Steady and Dynamic Behavior of Transverse Liquid Jets (2007).
14. Elshamy O, Tambe S, Cai J, Jeng S-M. Excited Liquid Jets in Subsonic Crossflow. In: *45th AIAA Aerospace Sciences Meeting and Exhibit* (2007). doi:10.2514/6.2007-1340
15. Deepe J, Lee J, Santavicca D, Lee W. *Effect of Weber Number on Modulated Jets in Crossflow*. Amsterdam, Netherlands: Elsevier Inc. (2006). doi:10.2514/6.2006-1223
16. Lee I, Kang Y, Moon H, Jang SP, Kim JK, Koo J. Spray Jet Penetration and Distribution of Modulated Liquid Jets in Subsonic Cross-Flows. *J Mech Sci Technology* (2010) 24:1425–31. doi:10.1007/s12206-010-0418-0
17. Anderson T, Proscia W, Cohen J (2001). Modulation of a Liquid-Fuel Jet in an Unsteady Cross-Flow, 2. V002T02A015. doi:10.1115/2001-GT-0048
18. Shaw VG, Elliott P, Boller M, Shaffer KE, Gutmark EJ. Droplet Evaporation of Water and Fuel Jets in Low and High Temperature Subsonic Crossflows. *Exp Therm Fluid Sci* (2022) 135:110626. doi:10.1016/j.expthermflusci.2022.110626
19. Zhu Y, Xiao F, Li Q-L, Mo R, Li CP, Lin S. Les of Primary Breakup of Pulsed Liquid Jet in Supersonic Crossflow. *Acta Astronautica* (2019). 28(8):082101.
20. Liu N, Wang Z, Sun M, Deiterding R, Wang H. Simulation of Liquid Jet Primary Breakup in a Supersonic Crossflow Under Adaptive Mesh Refinement Framework. *Aerospace Sci Technology* (2019) 91:456–73. doi:10.1016/j.ast.2019.05.017
21. Heinrich M, Schwarze R. 3d-coupling of volume-of-fluid and Lagrangian Particle Tracking for Spray Atomization Simulation in Openfoam. *SoftwareX* (2020) 11:100483. doi:10.1016/j.softx.2020.100483
22. Bhatia B, Johny T, De A. Understanding the Liquid Jet break-up in Various Regimes at Elevated Pressure Using a Compressible VOF-LPT Coupled Framework. *Int J Multiphase Flow* (2023) 159:104303. doi:10.1016/j.ijmultiphaseflow.2022.104303
23. Sun Y, Li Y, Dreßler L, Nishad K, Sadiki A. Multiscale Numerical Modeling of a Complete Spray Evolution Including Breakup of Liquid Jet Injection in Gaseous Cross Flow. *Int J Multiphase Flow* (2024) 170:104655. doi:10.1016/j.ijmultiphaseflow.2023.104655
24. Sun Y, Hasse C, Sadiki A. Large Eddy Simulation Based Seamless VOF-LPT Approach for Describing Atomization and Evaporation Processes: Application to Jets in Crossflow. *Int J Heat Mass Transfer* (2025) 242:126807. doi:10.1016/j.ijheatmasstransfer.2025.126807
25. Zhou C, Zou J, Zhang Y. Effect of Streamwise Perturbation Frequency on Formation Mechanism of Ligament and Droplet in Liquid Circular Jet. *Aerospace* (2022) 9:191. doi:10.3390/aerospace9040191

26. Zou J, Zhao Z, Zhou C, Wei Y. Direct Numerical Simulation and Analysis of Perturbation Effects on Swirling Liquid Sheet. *Atomization and Sprays* (2025) 35:1–26. doi:10.1615/AtomizSpr.2025057661
27. Popinet S. Gerris: A Tree-Based Adaptive Solver for the Incompressible Euler Equations in Complex Geometries. *J Comput Phys* (2003) 190:572–600. doi:10.1016/S0021-9991(03)00298-5
28. Popinet S. An Accurate Adaptive Solver for Surface-Tension-Driven Interfacial Flows. *J Comput Phys* (2009) 228:5838–66. doi:10.1016/j.jcp.2009.04.042
29. Scardovelli R, Zaleski S. Direct Numerical Simulation of Free-Surface and Interfacial Flow. *Annu Rev Fluid Mech* (1999) 31:567–603. doi:10.1146/annurev.fluid.31.1.567
30. Bell JB, Colella P, Glaz HM. A Second-Order Projection Method for the Incompressible Navier-Stokes Equations. *J Comput Phys* (1989) 85:257–83. doi:10.1016/0021-9991(89)90151-4
31. Crank J, Nicolson P. A Practical Method for Numerical Evaluation of Solutions of Partial Differential Equations of the heat-conduction Type. *Math Proc Cambridge Philosophical Soc* (1947) 43:50–67. doi:10.1017/S0305004100023197
32. Shinjo J, Umemura A. Simulation of Liquid Jet Primary Breakup: Dynamics of Ligament and Droplet Formation. *Int J Multiphase Flow* (2010) 36:513–32. doi:10.1016/j.ijmultiphaseflow.2010.03.008
33. Yang X, Turan A. Simulation of Liquid Jet Atomization Coupled with Forced Perturbation. *Phys Fluids* (2017) 29:022103. doi:10.1063/1.4976621
34. Xiao F, Dianat M, McGuirk JJ. Large Eddy Simulation of Liquid-Jet Primary Breakup in Air Crossflow. *AIAA J* (2013) 51:2878–93. doi:10.2514/1.J052509
35. Eggers J, Villermaux E. Physics of Liquid Jets. *Rep Prog Phys* (2008) 71:036601. doi:10.1088/0034-4885/71/3/036601
36. Li X, Soteriou MC. High Fidelity Simulation and Analysis of Liquid Jet Atomization in a Gaseous Crossflow at Intermediate Weber Numbers. *Phys Fluids* (2016) 28:082101. doi:10.1063/1.4959290.082101
37. Cárdenas C, Suntz R, Denev J, Bockhorn H. Two-Dimensional Estimation of Reynolds-Fluxes and -Stresses in a Jet-In-Crossflow Arrangement by Simultaneous 2d-lif and Piv. *Appl Phys B* (2007) 88:581–91. doi:10.1007/s00340-007-2734-3
38. Chai X, Iyer PS, Mahesh K. Numerical Study of High Speed Jets in Crossflow. *J Fluid Mech* (2015) 785:152–88. doi:10.1017/jfm.2015.612
39. Eslamian M, Amighi A, Ashgriz N. Atomization of Liquid Jet in High-Pressure And High-Temperature Subsonic Crossflow. *AIAA J* (2014) 52:1374–85. doi:10.2514/1.J052548